ACI MATERIALS JOURNAL TECHNICAL PAPER

Title no. 106-M56

Acoustic Emission and Ultrasound for Damage Characterization of Concrete Elements

by Dimitrios G. Aggelis, Tomoki Shiotani, Shouhei Momoki, and Akinobu Hirama

The acoustic emission (AE) technique is widely used for real time damage detection in concrete. It uses stress waves emerging from nucleation and propagation of cracks recorded on the surface of the material by suitable sensors. In the present study, AE is used to monitor the deterioration progress of reinforced concrete beams subjected to four-point bending. The specimens consist of two layers of plain and fiber concrete. At different loading steps, ultrasonic pulse velocity measurements were also conducted to obtain the transient three-dimensional tomographic reconstruction of the internal structure. The AE source location is in good agreement with the velocity structure visualization and the results are confirmed by visual observation of the actual cracks developed. The results show that the AE technique and velocity tomography are useful tools to study the failure progress of concrete.

Keywords: acoustic emission; cracking; fiber reinforcement; four-point bending; tomography.

INTRODUCTION

Stress wave techniques, such as acoustic emission (AE) and ultrasonic pulse velocity (UPV) have been used for many decades to study the fracturing behavior of cementitious materials. AE uses the transient waves that are emitted by the initiation and propagation of cracks when the material is under stress. These transient waves (AE signals) are detected by AE sensors attached to the surface of the material. The source of the transient signals is an AE "event" that is related to the fracture process (for example, one crack nucleation or propagation incidence). One event leads to a stress wave propagating in all directions, which is recorded almost simultaneously by different sensors. Analysis of the wave characteristics and the origin can provide useful information about the internal condition of the structure. The advantage of AE is the recording of the damage process during the entire load history, which enables determination of the onset of fracture and tracking of all subsequent failure stages. In several studies, AE parameters have been correlated with the failure modes, such as the drying shrinkage cracking of fresh concrete,[1] the damage evolution under bending test,[2-5] pullout,[6] and splitting tests.[7] Specific AE indexes have been used to identify the moment of critical failures[8,9] much earlier than visual observation or drop of mechanical load readings. Therefore, AE is employed in the monitoring of full-scale structures like bridges,[10] railway concrete piles,[11,12] dams,[13] and land slide monitoring.[14]

Another technique that has been used for concrete nondestructive testing for many decades is UPV. Pulse velocity has been correlated with strength[15,16] and damage[17,18] of concrete materials, offering rough but valuable estimations because the damage condition influences the mechanical properties and, hence, the wave speed. Employing a number of sensors, the velocity structure of the material can be constructed and the internal condition can be visualized, highlighting the existence of voids or cracks.[19-21]

In the present case, the aforementioned techniques are both used to study the fracture behavior of concrete specimens. Two different types of specimens were tested; namely, plain concrete and two-layered (concrete on top and vinyl fiber-reinforced mortar at the bottom) to investigate the differences in structural behavior. It is mentioned that the selection of the materials was motivated by a tunnel repair project where the deteriorated surface layer was removed and replaced by a shotcreted vinyl fiber mortar that was placed along with a metal lattice. Both techniques can be used for any other type of specimen.

RESEARCH SIGNIFICANCE

Deterioration of old concrete structures is a worldwide concern. The evaluation of the structural condition by means of nondestructive testing (NDT) techniques should be improved in terms of accuracy and reliability. The application of two complementary techniques (AE and UPV) can validate the results individually obtained. In laboratory conditions, visual observation can confirm the findings (for example, location of the actual cracks on the specimen compared to the AE sources). In large structures, however, visual observation is not always possible, and, therefore, development of reliable NDT techniques is highly desirable. Simultaneous use of different techniques aided by visual inspection is a step toward reliable examination of large structures.

EXPERIMENTAL PROCEDURE—MATERIALS

The mechanical loading was conducted by means of a four-point bending configuration. A typical specimen is depicted in Fig. 1. The dimensions were 150 x 150 x 530 mm (5.9 x 5.9 x 20.9 in.). Two reinforcing bars D13 (diameter of 13 mm [0.51 in.]) were installed 30 mm (1.18 in.) from the bottom. For one type of specimen, plain concrete was used with a maximum aggregate size of 25 mm (0.98 in.). The water-cement ratio (w/c) was 0.5 by mass and the aggregate-to-cement ratio was 3.6. As for the composite specimens, the top layer was plain concrete and the bottom layer (half of the thickness) was vinyl fiber-reinforced mortar. The fibers were 12 mm (0.47 in.) long and 0.5 mm (0.02 in.) thick and were used in a volume percentage of 0.5%. Seven days after the concrete layer was cast, the fiber mortar was cast on top. The reason for this waiting period was that in the actual application, the fiber mortar would be shot on top of fully hardened

ACI Materials Journal, V. 106, No. 6, November-December 2009.
MS No. M-2008-320.R1 received February 23, 2009, and reviewed under Institute publication policies. Pertinent discussion including authors' closure, if any, will be published in the September-October 2010 *ACI Materials Journal* if the discussion is received by June 1, 2010.

Dimitrios G. Aggelis *is an Assistant Professor in the Materials Science and Engineering Department at the University of Ioannina, Ioannina, Greece. He received his diploma in mechanical engineering from the University of Patras, Rio Patras, Greece, and his PhD in nondestructive testing of concrete from the same institute. His research interests include concrete damage characterization using stress wave propagation techniques.*

Tomoki Shiotani *is an Associate Professor at the Graduate School of Engineering at Kyoto University, Kyoto, Japan. He received his BS and MSc from the Civil Engineering Department of University of Tokushima, Tokushima, Japan, and his PhD from the Civil Engineering Department of the University of Kumamoto, Kumamoto, Japan. His research interests include damage characterization using stress waves, for example, acoustic emission and tomography.*

Shouhei Momoki *is a Research Engineer at the Research Institute of Technology, Tobishima Corporation, Noda, Japan. He received his master's degree in agricultural engineering from the University of Kyoto. His research interests include damage monitoring and structural health condition evaluation of civil structures using nondestructive testing.*

Akinobu Hirama *is the Manager of the Materials Laboratory of the Research Institute of Technology, Tobishima Corporation, Noda, Japan. He is a Civil Engineer from Nihhon University, Tokyo, Japan. His research interests include shotcrete, coal ash, maintenance, and repair of concrete structures.*

concrete and, therefore, no strong chemical bond between the layers was expected. It is mentioned that during the bending experiment, the fiber mortar layer, which included the reinforcing bars, was at the bottom, tensile side. Two specimens of each type were tested in bending.

AE AND PULSE VELOCITY MEASUREMENTS

Twelve 60 kHz resonant AE sensors were attached on the surfaces of the specimens (refer to Fig. 1). When the sensors are hit by a wave (due to cracking or another reason), the pressure on their surface is converted to electric voltage due to the piezoelectric effect. If this voltage was beyond the threshold (40 dB in our case), the signal was preamplified by another 40 dB digitized and stored in a 16 channel system with a sampling rate of 1 MHz. The software, in cooperation with the acquisition board, enables the calculation of major parameters of the signal like its amplitude, duration, and frequency in real time. These parameters are automatically extracted and stored for each of the thousands of individual signals recorded during the experiment. Apart from the post-analysis of parameters and waveforms, the software provided a real-time event source location during the experiment for the events recorded by at least six sensors. The range of frequencies of typical hits in this experiment lies between 20 and 100 kHz.

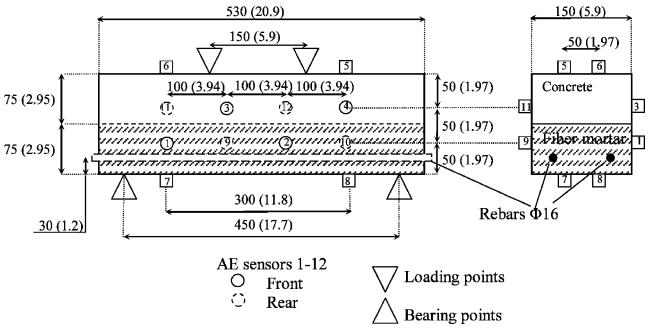

Fig. 1—Specimen geometry and sensor location. Dimensions are in mm (in.).

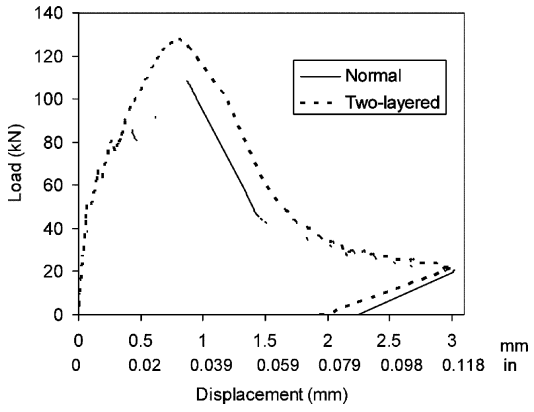

Fig. 2—Load versus central deflection for different types of specimens.

To conduct velocity measurements, the load was held at certain successive levels. During the pause, pencil lead break excitation was conducted near each sensor and the transient responses of the rest of the sensors were measured. The introduced band of frequencies is up to 200 kHz and, thus, the sensors of 60 kHz resonance are certainly within the range. The typical wavelengths collected by the sensors after excitation by the pencil are approximately 45 to 70 mm (1.77 to 2.76 in.). The transit time and pulse velocity could be calculated for all the combinations of wave paths among the different sensors. This information was entered into a suitable tomography program,[19] leading to the three-dimensional velocity structure of the specimen at each different loading stage. The software used herein has been applied in several cases in recent literature[13,19-21] and the interested reader is directed for more details elsewhere.[19] The following major points can be mentioned briefly: the structure or specimen under examination is divided into cubic cells. When the ultrasonic measurements are completed, a large number of paths inside the structure have been examined (all possible combinations of paths between the transducers). For each cell, there are a number of wave paths passing through it, depending on the cell position and the position of the sensors. The average of the pulse velocities of these paths (which is directly measured at the UPV experiment) is assigned to the specific cell. In case a defect exists inside a specific cell, it is reasonable that the wave paths passing through this cell will exhibit lower pulse velocities than others. Thus, from the first step of the procedure there are some discrepancies according to the actual damage pattern. To improve accuracy, iterative procedures are implemented to compensate for the fact that in the presence of damage, the wave does not always propagate in a straight line.

RESULTS

The main purpose of this study is the application of two NDT techniques for damage characterization. Before the presentation of the main results, however, it is worth showing the mechanical behavior of the specimens. In Fig. 2, one can see the load versus the midspan vertical displacement curves for the different types of specimens. A certain amount of extra strength is supplied by the fibers, because the maximum load increased by 19% compared to plain concrete (129.8 kN and 109.1 kN, respectively). The total absorbed energy, however, was only slightly increased, as can be seen by the area under the curve.

AE behavior

Concerning the interpretation of AE results, there are many possible wave source origins, such as matrix micro-cracking, friction in aggregates and metal reinforcing bars,

fiber pull-out and breakage, or macro-cracks in the matrix. Therefore, the characterization of the AE signals in concrete structures is not always straightforward.[3,6] A lot of information can be exploited, however, by the use of specific indexes concerning the severity of the situation.

Total AE activity

In Fig. 3(a), one can see the time history of the applied load along with the acoustic emission events for plain concrete. The step loading was applied to enable pulse velocity measurement at different load levels, which will be described later. The number of AE events started to increase rapidly during the third load stage (or approximately 35% of the ultimate load, at approximately 600 seconds), meaning at that time intensive cracking phenomena occurred. It must be noted that as the maximum load is approached, the specimen progressively becomes severely cracked and, therefore, acquisition of signals is hindered by the discontinuities. Thus, the total number of events is expected to be higher than recorded.

In Fig. 3(b), one can see the time history for the composite specimen. The major event outburst comes at the fourth stage (or approximately 50% of the ultimate load, after 700 seconds). This delay is attributed to the fiber action that restrained the early cracking of the material. Additionally, the total number of events was substantially lower in this case (1777 compared to the 5540 events of the plain concrete).

I*b*-value

It is reasonable that as the load increases, larger-scale fracture events occur. These give rise to AE events of larger amplitude. At the same time, however, the accumulated damage increases the attenuation of the material, making the study of the amplitude solely misleading. Therefore, the amplitudes are studied by their cumulative distribution, using the improved I*b*-value analysis.[8] This index (I*b*-value) takes into account the number of recent events and their amplitude range. It expresses the slope of the cumulative amplitude distribution as illustrated in Fig. 4(a). For a population of recent events (that is, 100 in this case), assuming an average amplitude μ and a standard deviation σ of the amplitudes, the I*b*-value was calculated as

$$Ib = \frac{\log_{10}N(\mu - \sigma) - \log_{10}N(\mu + \sigma)}{2\sigma} \quad (1)$$

where $N(\mu - \sigma)$ is the number of hits with an amplitude higher than $\mu - \sigma$, and $N(\mu + \sigma)$ is the number of hits with an amplitude higher than $\mu + \sigma$. According to the cumulative amplitude distribution, the index (I*b*-value) changes, following the fracture progress. It has been confirmed that as the fracture phenomena become more intense, the percentage of strong events increases relative to the weak ones in the total population. Therefore, the absolute gradient of this distribution (or I*b*-value) exhibits abrupt drops[5,8,12] (Fig. 4(a)). The I*b*-values calculated during the whole process for the two types of experiments are depicted in Fig. 3(c) and (d). The first values of Fig. 3(c) correspond to the first hits recorded (before 400 seconds). After a sufficient population of hits (hits due to the bending process) is built, it is reasonable that the I*b*-values exhibit their maximum throughout the whole process at that point because the damage is still minor. In Fig. 3(c), at the early part of the history, the curve ranges from 0.06 to 0.12, while at the end of the second loading stage (approximately 400 seconds), the I*b*-value has dropped to 0.05 (refer to the arrow). At the start of the third step (approximately 600 seconds), new hits emerge and result in oscillations of the I*b*-value. It is noteworthy that during the load increasing steps, there are many oscillations, but the range and average value decreases from step to step. Specifically for the second step, as mentioned previously, the oscillations range between 0.06 and 0.12, while for the last step before failure, the oscillations are between 0.03 and 0.06. Although the I*b*-value is sensitive to damage, it does not necessarily decrease monotonically. The reason is that as the cracks propagate they encounter healthy material. When this healthy material starts to rupture, it gives

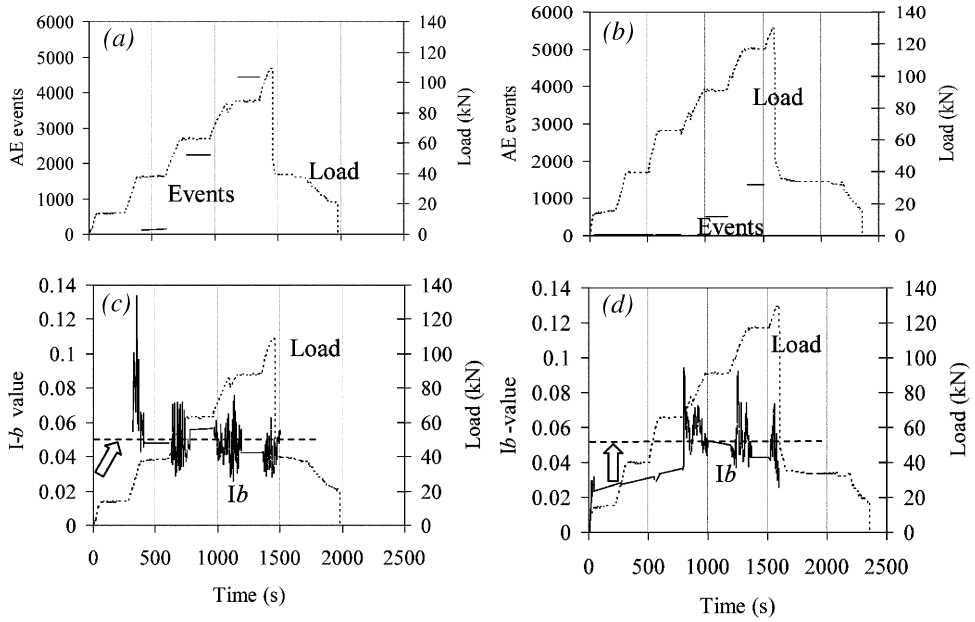

*Fig. 3—Step load and event time history for: (a) normal concrete; and (b) two-layer fiber concrete. Step load and I*b*-value for: (c) normal concrete; and (d) two-layer fiber concrete.*

signals corresponding to early damage, which are mixed with the signals of the already heavily damaged part. The most important parameters that should be read by the I*b*-value graph are the general trend of the curve and the minima obtained through the process. For the composite fiber specimen, the first noticeable decrease of the I*b*-value occurred after 50% of the maximum load (at approximately 800 seconds [refer to the arrow in Fig. 3(d)]). This is another confirmation that the fibers constrained the early fracturing phenomena for the composite. Among the drops that indicate fracture incidents, values less than 0.05 are correlated with a high degree of damage in the aforementioned literature. This value is reached very quickly for the plain mortar (just after the second loading stage [refer to the arrow in Fig. 3(c)]). On the contrary, this level is reached at the fourth stage for fiber mortar (Fig. 3(d)), while at earlier stages, the number of events is not sufficient for the I*b*-value calculation. Concerning the number of events included in the calculation, if the number is less than 50, then the oscillations are too strong, masking the general trend. On the other hand, if the number is too large, any small incidence producing just a small number of events would be undermined in the average of the large population. Thus, it is advised in literature to use either 50 or 100 hits.[8] In this case, a number of 100 events was used.

Other AE characteristics

It is accepted that nucleation of shear cracks follows nucleation of tensile cracks during the fracture process.[14,22] In any case, it can be confirmed that the final macroscopic fracture is formed by visible shear cracks that start near the support of the specimen on the bottom surface and develop at an angle of approximately 45 degrees to the top. For signals originating from shear events, the time delay between onset and the peak amplitude, called rise time (RT), is longer (refer to Fig. 4(b))[10,14] whereas the amplitude may also be higher. In Fig. 5(a), the average RT of the waveforms for different stages is presented. Concerning the normal specimen, RT increases continuously until fracture. For the composite specimen, RT also increases but in much lower levels. Figure 5(b) shows the average grade of the waveforms, which is simply the waveform amplitude divided by RT[14] expressed in *dB*/μσ. It is obvious that the grade is lower for plain concrete. According to literature,[8,14] this again shows that shear effects are stronger and progressively dominate the fracture behavior in the plain concrete specimen. It is mentioned that the grade is first calculated for each single event and subsequently averaged for the total number of events of each loading stage to produce the curves of Fig. 5(b).

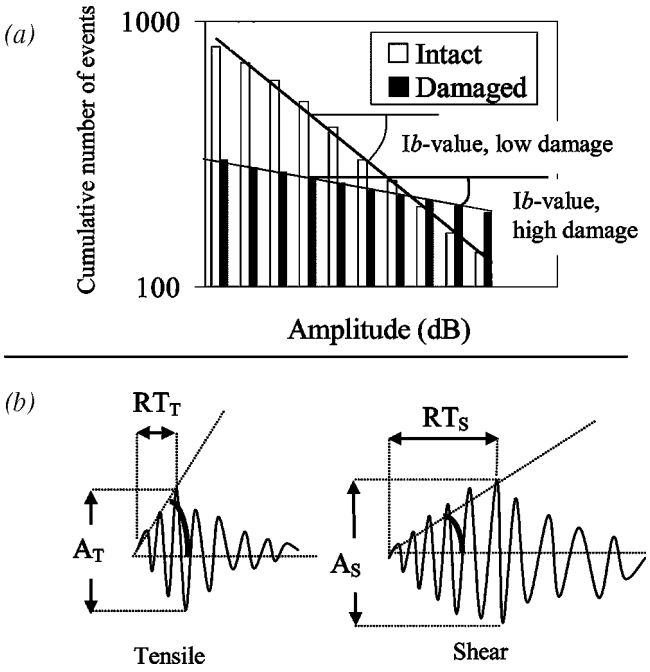

Fig. 4—(a) AE amplitude distribution; and (b) typical AE signals due to different types of fracture.

AE location

Due to the configuration of the experiment, the tensile surface is at the bottom of the specimen. Therefore, it is reasonable that the crack initiation occurs close to the bottom surface. This is revealed by Fig. 5(c), where the average height of the event initiations is depicted for different loads. At the lowest load level, the average location of the events is close to the bottom surface (40 mm [1.57 in.] for plain concrete and 27 mm [1.06 in.] for the composite). As the cracks propagate to the top, the AE sources naturally translate to higher locations, reaching 80 mm (3.15 in.) and 90 mm (3.54 in.) for the plain and the composite specimen, respectively.

Examples of the determined locations of the events for specific load stages are depicted in Fig. 6 for the two specimens. In the same figure, the observed cracks after final failure are

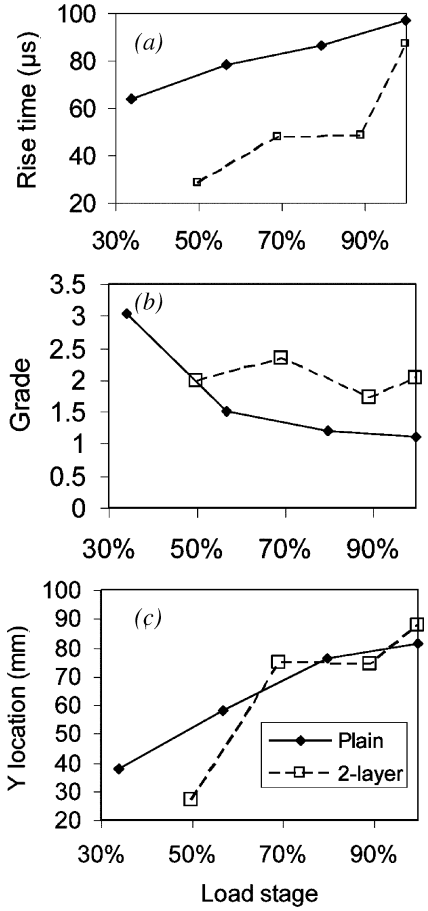

Fig. 5—(a) rise time; (b) grade; and (c) average height of localized events for different loading stage for both specimens. (Note: 1 mm = 0.0394 in.)

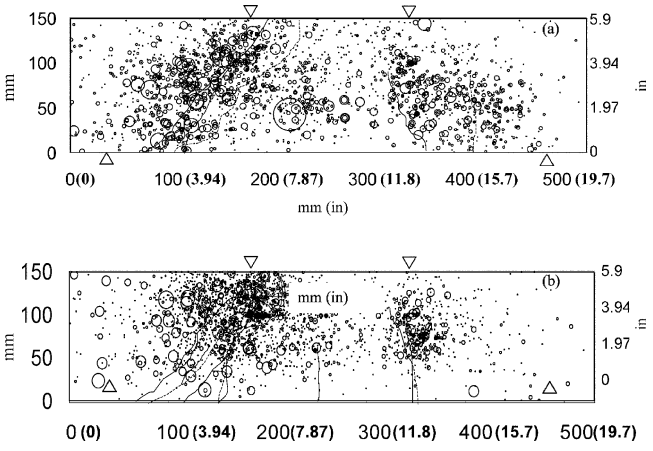

Fig. 6—Location of AE events and actual pattern of cracks for: (a) plain concrete specimen at third loading stage; and (b) composite specimen at fifth stage. (Solid line: front view, dash line: rear view.)

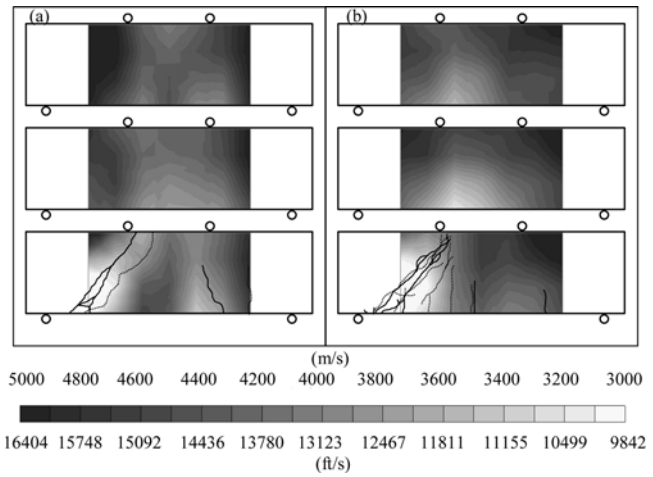

Fig. 7—Velocity tomography of central cross section of: (a) plain concrete; and (b) two-layer specimen for different loading stages. From top to bottom: initial condition, approximately 50% and 90% of final load.

also depicted. The events are represented by circles whose center is the determined location of the source and their area is proportional to their amplitude. Figure 6(a) concerns the plain concrete specimen during loading from 57 to 80% of the ultimate load (the fourth stage of loading in Fig. 3(a)). A great number of events are localized near the system of large diagonal cracks at the left. Also, the smaller crack at the right part is accompanied by numerous events, which are located to the right of the crack. It is mentioned that the development of cracks hinders the acquisition of all signals. Severe scattering imposes attenuation and delay to the acquisition of individual signals, and therefore for severely damaged material the accuracy of location is expected to decrease.[2]

Concerning the two-layer composite specimen (Fig. 6(b)) during loading from 89% to maximum load (sixth stage of Fig. 3(b)), one can clearly see the accumulation of events near the edge of the diagonal crack developing from the left, as well as other events near the tip of a smaller crack propagating vertically towards the top surface, at the horizontal location of approximately 350 mm (13.78 in.).

It is worth mentioning that no delaminations occurred in the two-layer composite specimens. The final fracture pattern was similar to the one of plain concrete (development of diagonal cracks from the bottom to the top surface). This shows that although the second layer was cast several days later on top of the first, the bond between them was still adequate.

TOMOGRAPHY RESULTS

In concrete literature, it is well known that low pulse velocity is indicative for the damage.[15-18] The correlations are rough; however, velocities of approximately 4000 m/second (13,123 ft/second) or higher imply quite healthy material, while those lower than 3000 m/second (9843 ft/second) are indicative of a troublesome condition. Using the same sensors and positions that were used for the AE testing, the transit times of different paths were measured at different instances during the loading. The values were fed to suitable software[19] and the three-dimensional velocity structure of the specimen was constructed for different stages. Tomography results based on the pulse velocity are depicted in Fig. 7 for the two types of specimens and different loading stages. The top graphs correspond to the intact condition and the next two to the last two loading stages for the central cross section of the specimens.

At the intact condition, the velocity at any area of the materials is more than 4000 m/second (13,123 ft/second). During the initial load stages, velocity seems to decrease near the bottom surface because of crack initiation due to tensile load. At the final stage, the development of the large scale cracks influence the velocity more critically. Pulse velocity decreases to 3000 m/second (9843 ft/second) at the zone where the diagonal macroscopic cracks developed.

It is mentioned that due to the arrangement of the sensors, the tomography cell size is quite coarse (50 mm [2 in.]). Additionally, using the velocity of intact material (approximately 4500 m/second [14,764 ft/second]), the major wavelength is on the order of 40 to 70 mm (1.57 to 2.75 in.). Considering also the cell size, it is realized that the accuracy is compromised. Areas of the specimens containing dense cracks, however, are identified correctly (see the left part of both tomograms at the bottom of Fig. 7), while the changes due to increasing deterioration at each stage are evident. The accuracy can be enhanced by increasing the number of sensors and the frequency of the test.

CONCLUSIONS

In the present paper, AE and ultrasonic techniques (UT) are used to follow the fracture behavior of different types of cementitious specimens. It is seen that the combination of fiber mortar and concrete in a two-layer specimen exhibits higher strength than a plain concrete specimen of the same cross section. Study of the AE characteristics showed that as the load increases, shear effects dominate the fracture behavior. In any case, the ultimate failure was accompanied by macroscopic shear diagonal cracks. The basic conclusions are summarized in the following:

1. Vinyl fibers seem to delay the onset of macroscopic fracturing, as revealed by the AE behavior, offering extra strength to the material.

2. AE event locations and low UPV areas coincide to a great extent with the visually-observed cracks. This shows the reliability of the techniques, which can be used in large structures where visual observation is not always possible.

3. AE and UPV work complementary to each other: small cracks that cannot influence pulse velocity can be identified by AE as they propagate. On the other hand, inactive cracks that show no AE activity influence UPV and can be detected.

4. Simultaneous application of stress wave techniques (AE and UT) shows the ability to identify the time and location of cracking and offer a general assessment for the deterioration condition of the material.

REFERENCES

1. Shiotani, T.; Bisschop, J.; and Van Mier, J. G. M., "Temporal and Spatial Development of Drying Shrinkage Cracking in Cement-Based Materials," *Engineering Fracture Mechanics*, V. 70, No. 12, 2003, pp. 1509-1525.

2. Schechinger, B., and Vogel, T., "Acoustic Emission for Monitoring a Reinforced Concrete Beam Subject to Four-Point-Bending," *Construction and Building Materials*, V. 21, No. 13, 2007, pp. 483-490.

3. Wu, K.; Chen, B.; and Yao, W., "Study on the AE Characteristics of Fracture Process of Mortar, Concrete, and Steel-Fiber-Reinforced Concrete Beams," *Cement and Concrete Research*, V. 30, 2000, pp. 1495-1500.

4. Chen, B., and Liu, J., "Experimental Study on AE Characteristics of Three-Point-Bending Concrete Beams," *Cement and Concrete Research*, V. 34, 2004, pp. 391-397.

5. Kurz, J. H.; Finck, F.; Grosse, C. U.; and Reinhardt, H. W., "Stress Drop and Stress Redistribution in Concrete Quantified Over Time by the B-Value Analysis," *Structural Health Monitoring*, V. 5, 2006, pp. 69-81.

6. Grosse, C.; Reinhardt, H.; and Dahm, T., "Localization and Classification of Fracture Types in Concrete with Quantitative Acoustic Emission Measurement Techniques," *NDT&E International*, V. 30, No. 4, 1997, pp. 223-230.

7. Grosse, C. U., and Finck, F., "Quantitative Evaluation of Fracture Processes in Concrete using Signal-Based Acoustic Emission Techniques," *Cement and Concrete Composites*, V. 28, No. 4, 2006, pp. 330-336.

8. Shiotani, T.; Fujii, K.; Aoki, T.; and Amou, K., "Evaluation of Progressive Failure using AE Sources and Improved B-value on Slope Model Tests," *Progress in Acoustic Emission*, V. 7, 1994, pp. 529-534.

9. Colombo, S.; Forde, M. C.; Main, I. G.; and Shigeishi, M., "Predicting the Ultimate Bending Capacity of Concrete Beams from the 'Relaxation Ratio' Analysis of AE Signals," *Construction and Building Materials*, V. 19, 2005, pp. 746-754.

10. Ohtsu, M.; Uchida, M.; Okamoto, T.; and Yuyama, S., "Damage Assessment of Reinforced Concrete Beams Qualified by Acoustic Emission," *ACI Structural Journal*, V. 99, No. 4, July-Aug. 2002, pp. 411-417.

11. Shiotani, T.; Nakanishi, Y.; Iwaki, K.; Luo, X.; and Haya, H., "Evaluation of Reinforcement in Damaged Railway Concrete Piles by Means of Acoustic Emission," *Journal of Acoustic Emission*, V. 23, 2005, pp. 260-271.

12. Shiotani, T.; Nakanishi, Y.; Luo, X.; Haya, H.; and Inaba, T., "Damage Evaluation for Railway Structures by Means of Acoustic Emission," *Key Engineering Materials*, V. 270-273, 2004, pp.1622-1630.

13. Shiotani, T., and Aggelis, D. G., "Evaluation of Repair Effect for Deteriorated Concrete Piers of Intake Dam Using AE Activity," *Journal of Acoustic Emission*, V. 25, 2007, pp. 69-79.

14. Shiotani, T.; Ohtsu, M.; and Ikeda, K., "Detection and Evaluation of AE Waves due to Rock Deformation," *Construction and Building Materials*, V. 15, No. 5-6, 2001, pp. 235-246.

15. Kaplan, M. F., "The Effects of Age and Water/Cement Ratio upon the Relation between Ultrasonic Pulse Velocity and Compressive Strength," *Magazine of Concrete Research*, V. 11, No. 32, 1959, pp. 85-92.

16. Popovics, S., "Analysis of the Concrete Strength versus Ultrasonic Pulse Velocity Relationship," *Materials Evaluation*, V. 59, No. 2, 2001, pp. 123-130.

17. Ono, K., "Damaged Concrete Structures in Japan due to Alkali Silica Reaction," *The International Journal of Cement Composites and Lightweight Concrete*, V. 10, No. 4, 1988, pp. 247-257.

18. Van Hauwaert, A.; Thimus, J. F.; and Delannay, F., "Use of Ultrasonics to Follow Crack Growth," *Ultrasonics*, V. 36, 1998, pp. 209-217.

19. Kobayashi, Y.; Shiotani, T.; Aggelis, D. G.; and Shiojiri, H., "Three-Dimensional Seismic Tomography for Existing Concrete Structures," *Proceedings of the Second International Operational Modal Analysis Conference*, IOMAC 2007, (April 30-May 2, 2007, Copenhagen), V. 2. pp. 595-600.

20. Aggelis, D. G., and Shiotani, T., "Repair Evaluation of Concrete Cracks using Surface and through-Transmission Wave Measurements," *Cement and Concrete Composites*, V. 29, No. 9, 2007, pp. 700-711.

21. Aggelis, D. G., and Shiotani, T., "Damage Characterization of Deteriorated Concrete Structures by Stress Wave Methods," *Emerging Technologies in NDT*, (ETNDT 4), April 2-4, 2007, Stuttgart (CD-ROM).

22. Farid Uddin, A. K. M.; Numata, K.; Shimasaki, J.; Shigeishi, M.; and Ohtsu, M., "Mechanisms of Crack Propagation due to Corrosion of Reinforcement in Concrete by AE-SiGMA and BEM," *Construction and Building Materials*, V. 18, 2004, pp. 181-188.